

Image Reconstruction for Three-Dimensional Transmitted-Light DIC Microscopy

Chrysanthe Preza†, Donald L. Snyder†, José-Angel Conchello
Institute for Biomedical Computing
and †Department of Electrical Engineering
Washington University, St. Louis, Missouri

ABSTRACT

The derivation of an iterative method for phase reconstruction from Differential-Interference-Contrast (DIC) images is presented here. Because DIC imaging is direction sensitive, in our approach we estimate a specimen's phase function using multiple DIC images obtained by rotating the specimen. Results obtained from testing the method via two-dimensional simulations demonstrate that the use of multiple DIC images at different specimen rotations yield phase reconstructions that more closely resemble the phase function of phantoms than the unprocessed DIC images. Improvement in resolution was also achieved: two points separated by half the Rayleigh resolution limit for coherent illumination not resolved in the unprocessed DIC image, were successfully resolved in the reconstructed phase images. Our results show that phase reconstructions are quantitatively better and resolution is improved when two or more DIC images are used in the reconstruction.

Keywords: Computational Nomarski DIC microscopy, image reconstruction, 3D microscopy

1. INTRODUCTION

Nomarski Differential-Interference-Contrast (DIC) microscopy¹ is an important imaging modality for several reasons. First, it is widely used both in motility analysis and, more generally, for structural studies of biological specimens.² Second, it is particularly advantageous for time-lapse studies because it is not limited by photobleaching problems as with fluorescence microscopy. A unique feature of DIC microscopy is that it can be used to image transparent specimens not visible with ordinary transmitted-light microscopy without staining. In some cases, staining is toxic to living specimens and cannot be used. Furthermore, DIC microscopy can be used in combination with fluorescence microscopy^{3,4} to prevent photobleaching while searching for a region of interest and, also, to provide landmarks of cell or organ structure (images obtained with fluorescence microscopy often lack such landmarks because fluorescence dyes label only particular parts of a specimen).

In a DIC microscope, a two-dimensional (2D) image is formed from the interference of two mutually coherent waves that have a lateral differential displacement of a few tenths of a micrometer, called the *shear*, and are phase-shifted relative to each other.⁵ The phase difference between the two waves is due to variations in the refractive index across the specimen and, also, due to a uniform phase, called the *bias retardation*, which is a system parameter adjusted to increase contrast in DIC images. Because phase variations are converted to intensity variations with DIC imaging, differences in the refractive index of neighboring points in a specimen can be visualized as intensity variations in a DIC image. Thus, the intensity in the detected DIC images is approximately the derivative of the specimen's refractive index distribution along the direction of shear (perpendicular to the optical axis). This property of DIC imaging makes the interpretation of DIC images difficult and creates a shadow-cast effect in DIC images which gives a false three-dimensional (3D) impression. Clearly, DIC images are sensitive to the orientation of specimen features with respect to the direction of shear. As in any microscopical modality, the resolution in DIC images is degraded by the blurring effects of the microscope's objective lens.

In order to obtain an estimate of the specimen's refractive index distribution from DIC images, we have formulated an image reconstruction problem for DIC microscopy. Because DIC image formation is nonlinear, a closed form solution for this problem is not possible. Thus, we attempt to estimate the refractive index distribution

whose calculated DIC image “best” matches the measured DIC image. This requires an imaging model that will predict the measured DIC image from a specimen’s refractive index distribution. To this end, we have developed such a model for DIC imaging which was presented in a previous publication.⁶ The objective of our method is to obtain a quantitative estimate of the spatial index of refraction variations of the specimen, which is more fundamental than the gradient of the refractive index that is produced directly with the microscope and which microscope users normally view.

In this paper, we present an iterative method for the reconstruction of a specimen’s phase function from DIC images. The paper is organized as follows. Section 2. summarizes related work. In Section 3., a conjugate gradient method that solves the reconstruction problem is derived. Section 4. describes simulation studies performed to test the method’s ability to reconstruct phase functions from DIC images of simple phantoms. Finally, Section 4.2. summarizes results obtained from simulations.

2. RELATED WORK

In contrast to fluorescence microscopy, computational image-processing has not been applied to DIC microscopy. There are two reasons for this: 1, the lack of adequate imaging models for DIC microscopy; and 2, the difficulty in solving a nonlinear reconstruction problem. In the last decade there have only been a few attempts to develop reconstruction methods for DIC images. We briefly review related work below.

Holmes and Levy^{7,8} were the first to propose that a specimen’s phase function can be estimated from DIC images via computational methods. Their work was the first effort towards computational DIC and was developed for 2D DIC imaging. First, they derived an expression for the intensity of the DIC image for a 2D specimen. Using this expression and based on the Gerchberg-Saxton algorithm,⁹ Holmes and Levy developed an iterative algorithm to estimate a 2D phase function from a DIC image. Their results are encouraging because they show improvements in a synthetic DIC image (i.e. an image computed from a well-known computer-generated phantom) even in the presence of severe simulated additive Gaussian noise.⁸ However, these results are preliminary. First, their model was not tested by comparing model predictions to DIC images obtained from real phantom specimens. Second, the results were computed for only one bias setting (bias = -90 degrees) which provided a good initial guess for the algorithm. And third, to our knowledge, the method suggested by Holmes and Levy has not been applied to images from biological specimens.

The second effort towards computational DIC was by Dana,¹⁰ who developed a 3D linear model and used a Wiener Filter to deconvolve a specimen’s phase function. Dana was able to derive a linear model using several simplifying assumptions: 1, small refractive index variations across the specimen; 2, bias equal to 90 degrees; and 3, that the blurring due to the objective lens can be incorporated in the model by convolving the intensity point-spread function (PSF) with the intensity of the “ideal” DIC image derived without diffraction effects. However, the last assumption is not valid for DIC imaging in which diffraction effects must be incorporated by blurring the image amplitude with the amplitude PSF before the image intensity can be computed. This leads to a nonlinear model as we have shown in a previous publication.⁶ Because of this nonlinear image formation, a Wiener filter cannot be used to obtain the refractive index distribution from DIC images. Thus, the derived linear model and restoration method developed by Dana are inaccurate. The deficiency of the model is evident in the differences observed in Dana’s comparison of theoretical PSFs to images obtained from small beads ($0.24 \mu\text{m}$ in diameter) and in reconstructions of images obtained from larger beads ($4.6 \mu\text{m}$ in diameter). Dana noted that reconstructions showed improvements in images obtained from a biological specimen and that better results could be expected with a better model. In Dana’s work a method for calibrating the translation of the sliding Wollaston prism was also developed. This calibration provides the microscope’s bias retardation setting which is necessary for computational DIC.

3. IMAGE RECONSTRUCTION

Reconstruction methods have thus far found only limited application to DIC microscopy because of lack of imaging models. Our interest in developing a reconstruction method for transmitted-light DIC microscopy led us to the development of an imaging model described in detail elsewhere,⁶ which we summarize here for completeness.

The DIC-image intensity, $i(\mathbf{x})$, of a specimen characterized by a transmission function $f(\mathbf{x})$ and illuminated by a quasi-monochromatic source with a mean wavelength λ and intensity $a(\boldsymbol{\xi})$ (defined to have a zero value outside the circular aperture of the condenser lens) can be described by

$$i(\mathbf{x}) = \int_{-\infty}^{+\infty} a(\boldsymbol{\xi}) \left| \int_{-\infty}^{+\infty} f(\mathbf{x}_o) h(\mathbf{x} - \mathbf{x}_o) h_c(\boldsymbol{\xi}; \mathbf{x}_o) d\mathbf{x}_o \right|^2 d\boldsymbol{\xi}, \quad (1)$$

where $\boldsymbol{\xi} = [\xi, \eta]$, $\mathbf{x}_o = [x_o, y_o, z_o]$, and $\mathbf{x} = [x, y, z]$ denote points in the front-focal plane of the condenser lens, in the object plane, and in the image plane respectively, $h_c(\boldsymbol{\xi}; \mathbf{x}_o) = \frac{1}{j\lambda f_c} e^{j2\pi(x_o\xi + y_o\eta)/\lambda f_c}$, f_c is the focal distance of the condenser lens, and $h(\mathbf{x})$ is the DIC amplitude PSF. $h(\mathbf{x})$ can be expressed in terms of the coherent PSF, $k(\mathbf{x})$, which is defined as the Fourier transform of the pupil function (see Goodman,¹¹ p. 111):

$$h(x, y, z) = \frac{1}{2} \left[e^{-j\Delta\theta} k(x - \Delta x, y, z) - e^{j\Delta\theta} k(x + \Delta x, y, z) \right], \quad (2)$$

where $2\Delta\theta$ (expressed in radians) is the bias retardation setting, and $2\Delta x$ (expressed in length units) is the shear. The direction of shear, indicated here along the x axis without loss of generality, is perpendicular to the optical axis, z .

The problem of interest is: given one or more measured DIC images, estimate the function $f(\mathbf{x}_o)$ that is consistent with (1). Because $f(\mathbf{x}_o) = e^{-j\phi(\mathbf{x}_o)}$ for a nonabsorptive specimen, the estimation problem reduces to estimating the phase $\phi(\mathbf{x}_o)$ given the recorded images. Essentially, this is a phase-retrieval problem. Phase-retrieval problems in a number of other applications (such as estimation of turbulence-induced phase aberrations in phase-diverse speckle imaging) have been solved successfully using the concept of phase diversity.¹²⁻¹⁶ Phase diversity allows the estimation of an unknown phase aberration from two or more images obtained from the same scene by introducing a known amount of phase error. In an imaging system for example, one of these images could be the conventional focal-plane image that has been degraded by some unknown aberrations. Additional images of the same object can be recorded by translating the detector along the optical-axis. Due to the intentional translation, these images are further degraded by a known amount of defocus which is an example of one type of phase diversity.

Phase diversity in DIC data can be achieved by changing the bias retardation setting. We note that a DIC image obtained by changing the sign of the bias, but not the magnitude, can also be obtained by rotating the specimen (or the prisms and polarizers) by 180 degrees and leaving the bias unchanged. Because the DIC image is related to the directional derivative of the specimen's phase function along the direction of the shear, this *rotational diversity* provides information about the specimen-phase-function derivative in multiple directions. DIC images differing by 90 degree specimen rotation provide gradient information in two orthogonal directions. Although in theory four DIC images separated by a 90 degree rotation provide complete information of the gradient, in practice they do not due to the presence of detector and quantization noise. Thus, more images obtained at additional angles are useful, as they help to reduce the variance due to random noise (photon and camera noise) and may reduce the errors due to the finite sampling grid. Rotation of the prisms and polarizers instead of the specimen reduces the risk of misaligning the specimen with respect to the camera, and may be more suitable for *in vivo* specimen preparations. However, in most DIC microscopes the sliding Wollaston prism cannot be rotated and, thus, specimen rotation is dictated. This requires the use of a rotational stage available from several manufacturers.

In what follows, we first formulate a rotational-diversity model for DIC data, and based on this model we then derive a nonlinear least-squares optimization problem for which we obtain a solution using the conjugate gradient method. This is one possible reconstruction method that seems to be a reasonable first approach for the DIC phase-reconstruction problem, but other methods of numerical optimization may be useful as well.

3.1. Problem Statement

The rotation of the specimen about the optical axis can be added to the imaging formation model by incorporating the specimen's rotation in the model. The rotation can be modeled as part of the PSF by taking the

specimen coordinates as the reference for the rotation. This is equivalent to modeling rotation of the prisms and polarizers of the microscope, or rotation of the direction of shear for a fixed specimen. In what follows we use the terms “specimen rotation” and “shear rotation” without distinction.

Let γ_k be the rotation angle (taken to be positive for a counterclockwise rotation) of the shear direction for the k^{th} diversity image. Then the resulting PSF, $h_k(x, y, z)$, can be obtained from

$$h_k(x, y, z) = h(x' \cos \gamma_k + y' \sin \gamma_k, -x' \sin \gamma_k + y' \cos \gamma_k, z). \quad (3)$$

Using a finite-dimensional discrete version of (1) to represent the array of the k^{th} diversity image, i_k , and denoting by h_k the array of the PSF having diversity k , we write

$$i_k(\mathbf{x}) = \sum_{\boldsymbol{\xi} \in \Xi} \alpha(\boldsymbol{\xi}) \left| \sum_{\mathbf{x}_o \in \chi} f(\mathbf{x}_o) h_k(\mathbf{x} - \mathbf{x}_o) h_c(\boldsymbol{\xi}; \mathbf{x}_o) \right|^2, \quad (4)$$

where f is the object array with samples of $e^{-j\phi(\mathbf{x}_o)}$, $\alpha(\boldsymbol{\xi})$ and $h_c(\boldsymbol{\xi}; \mathbf{x}_o)$ are arrays that specify the illumination, and \mathbf{x} and \mathbf{x}_o are three-dimensional coordinates that take values on the set $\chi = \{0, 1, \dots, N-1\}^3$, and $\boldsymbol{\xi}$ takes values on $\Xi = \{0, 1, \dots, M-1\}^2$. The rotational-diversity images, $i_k(\mathbf{x})$ for $k = 0, \dots, K-1$, have a different shear direction depending on the rotation angle γ_k . In practice, the direction of shear is fixed in measured DIC images obtained by rotating a specimen, so measured images will have to be rotated computationally prior to further processing in order to account for this difference between the model and the measured data.

3.2. Optimization

The new reconstruction problem can now be stated: Given K rotational-diversity images d_k , $k = 0, \dots, K-1$, estimate the object’s phase function $\phi(\mathbf{x}_o)$. We seek a solution for the DIC reconstruction problem by minimizing the cumulative, uniformly weighted, squared-error,

$$E = \sum_{k=0}^{K-1} \sum_{\mathbf{x} \in \chi} [d_k(\mathbf{x}) - i_k(\mathbf{x})]^2, \quad (5)$$

between the measured images, $d_k(\mathbf{x})$, and the theoretical images, $i_k(\mathbf{x})$, predicted by the model in (4). Because of the nonlinear dependence of $i_k(\mathbf{x})$ on the specimen phase, an iterative method is required to obtain the solution that minimizes the cost function, E .

Let $\boldsymbol{\phi}$ be a vector having as elements the samples of the object’s phase function, $\phi(\mathbf{x}_o)$, to be estimated. An estimate of this vector can be obtained with the conjugate gradient method (see Aoki,¹⁷ p.118). This iterative method starts from some initial guess $\boldsymbol{\phi}^0$, and at iteration m it produces a new estimate for $\boldsymbol{\phi}$ by minimizing the cost function, E , along the direction, \mathbf{h}^m :

$$\begin{aligned} \boldsymbol{\phi}^{m+1} &= \boldsymbol{\phi}^m - \beta_m \mathbf{h}^m \quad m = 0, 1, \dots \\ \mathbf{r}^m &= \nabla E(\boldsymbol{\phi}^m), \\ \mathbf{h}^0 &= -\mathbf{r}^0, \\ \mathbf{h}^m &= -\mathbf{r}^m + \gamma_{m-1} \mathbf{h}^{m-1}, \\ \gamma_{m-1} &= \frac{\langle \mathbf{r}^m, \mathbf{r}^m \rangle}{\langle \mathbf{r}^{m-1}, \mathbf{r}^{m-1} \rangle}, \\ \beta_m &= -\frac{\langle \mathbf{r}^m, \mathbf{r}^m \rangle}{\langle \mathbf{r}^m, Q \mathbf{h}^m \rangle}, \end{aligned} \quad (6)$$

where β_m is the step size, Q is the Hessian matrix of the cost function, E , and $\langle \cdot, \cdot \rangle$ denotes the inner product operation. The elements of the gradient vector $\nabla E(\boldsymbol{\phi}^m)$ are:

$$\frac{\partial E}{\partial \phi^m(\mathbf{x}_o)} = 2 \sum_{k=0}^{K-1} \sum_{\mathbf{x} \in \chi} \frac{\partial i_k^m(\mathbf{x})}{\partial \phi^m(\mathbf{x}_o)} [i_k^m(\mathbf{x}) - d_k(\mathbf{x})], \quad (7)$$

where

$$\begin{aligned}\frac{\partial i_k^m(\mathbf{x})}{\partial \phi^m(\mathbf{x}_o)} &= 2 \operatorname{Im} \left[e^{-j\phi^m(\mathbf{x}_o)} h_k(\mathbf{x} - \mathbf{x}_o) a_k^m(\mathbf{x}; \mathbf{x}_o) \right], \\ a_k^m(\mathbf{x}; \mathbf{x}_o) &= \sum_{\mathbf{x}'_o \in \chi} e^{j\phi^m(\mathbf{x}'_o)} h_k^*(\mathbf{x} - \mathbf{x}'_o) j_s(\mathbf{x}_o; \mathbf{x}'_o), \\ j_s(\mathbf{x}_o; \mathbf{x}'_o) &= \sum_{\xi \in \Xi} \alpha(\xi) h_c(\xi; \mathbf{x}_o) h_c^*(\xi; \mathbf{x}'_o),\end{aligned}$$

$i_k^m(\mathbf{x})$ is the theoretical image obtained from $\phi^m(\mathbf{x}_o)$, $\operatorname{Im}[\cdot]$ is the operator that takes the imaginary part of its argument, and $*$ denotes the complex conjugate. Because it is not practical to evaluate the matrix Q , an estimate for the step size, β_m , is used in (6). This estimate is evaluated numerically at every iteration, to minimize the objective function in the direction h^m . The iterative procedure that we use to estimate β_m is based on the polynomial approximation method discussed by Aoki¹⁷ (p. 148). For a given h^m , three points of the cost function are evaluated so that they define an interval in which the cost function has a minimum. Because a parabola fitted through the three points yields the minimum of the cost function, the step size that corresponds to this minimum can be obtained by inverse parabolic interpolation.

We expect that the use of multiple DIC images at different specimen rotations will provide the necessary information needed so that the method can converge to a solution that is a global minimum of the cost function, but we have not yet proven this mathematically. In what follows we present results obtained from testing the method with simulations in order to assess its ability to reconstruct specimen-phase parameters from DIC images.

4. METHODS

In order to test the reconstruction method, we have performed simulations using synthetic-DIC images computed from our rotational-diversity model and computer-generated phantom specimens. For these simulations, we have used a special case of our imaging model which is based on coherent illumination (i.e. using a point condenser aperture).⁶ This imaging model case is evaluated from (4) with $\alpha(\xi) = \delta(\xi)$; this assumption considerably simplifies the equations for the reconstruction method that need to be implemented while still providing a good initial test for the reconstruction method. Images computed with this model compared well with actual DIC images acquired with a stopped-down condenser aperture as we showed in a previous publication.⁶

We have begun testing the reconstruction method with 2D simulations because effective 2D phase image-reconstruction is useful in its own right and, also, it is a prerequisite to 3D reconstruction. Furthermore, more rapid progress can be expected with 2D simulations, as fewer parameters need to be estimated than in a 3D simulation. We have used several very simple computer-generated phantoms for the simulations, and results from these are shown below.

4.1. Phantoms

Simple 2D computer-generated phantoms were created to resemble the 3D phantoms that we used for the imaging model validation published elsewhere.⁶ These phantoms consist of: 1, a disc (4 μm in diameter) with uniform refractive index $n_1 = 1.56$ embedded in a medium with refractive index $n_2 = 1.52$ (Figure 2a); and 2, two crossing bars (5 μm wide) with uniform refractive index $n_1 = 1.504$ embedded in a medium with uniform refractive index $n_2 = 1.494$ (Figure 6a). Additionally, a simple phantom that consists of two points was used to test the attainable resolution in the reconstructed images. The two points are each one pixel of refractive index $n_1 = 1.59$ separated by two pixels of the background refractive index $n_2 = 1.52$. This separation is equivalent to a distance of 0.68 μm , which is approximately half the Rayleigh resolution limit, $\rho = 0.82\lambda/N.A. = 1.5 \mu\text{m}$ (with $\lambda = 550 \text{ nm}$ and $N.A. = 0.3$), for coherent illumination (see Pluta,¹⁸ p.339).

The phase function of each phantom was obtained from the relation $\phi = 2\pi(n_1 - n_2)t/\lambda$, where t is the thickness of the phantom. This is a relative phase with respect to the background. It was assumed that the 2D phantoms

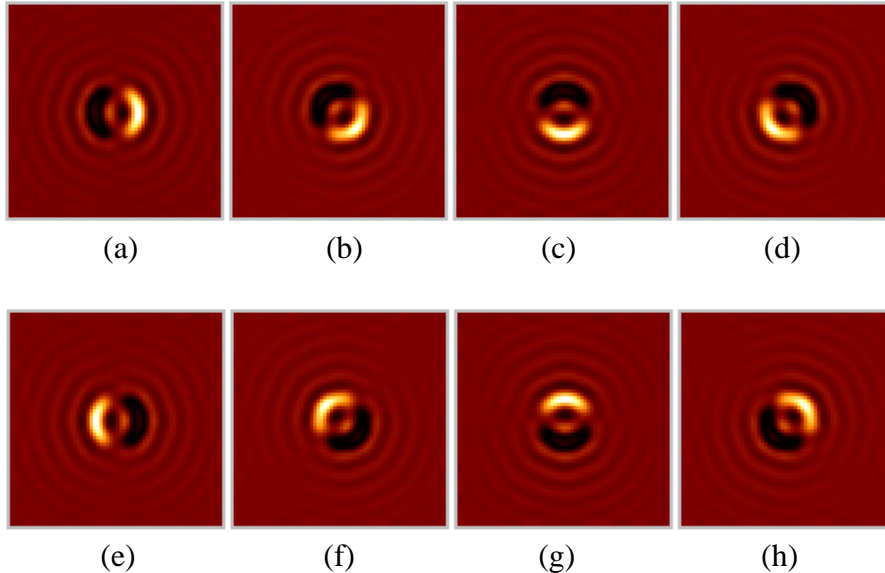


Figure 1: Synthetic rotational-diversity DIC images of a disc with uniform refractive index ($n_1 = 1.56$) embedded in a medium with refractive index $n_2 = 1.52$, with different orientation of the shear. The shear is along the horizontal axis in (a), and it is rotated every 45 degrees clockwise from (a) to (h).

have a small thickness of $1 \mu\text{m}$.

4.2. Simulations

Synthetic DIC images were generated using the phantoms described above and a 2D DIC PSF for a 10×0.3 N.A. lens. The DIC PSF was computed from (2), using a bias retardation of $2\Delta\theta = 0.3$ radians, and illumination wavelength, λ , equal to 550 nm. For each phantom, eight DIC images (Figure 1 and Figure 5) were generated using (3) and (4), for $\gamma_k = 0, \pm 45, \pm 90, \pm 135, 180$ degrees, and $\alpha(\xi) = \delta(\xi)$. Pixel arrays of dimension 64×64 were used, with pixel size $0.34 \mu\text{m} \times 0.34 \mu\text{m}$, for an overall image size of $22 \mu\text{m} \times 22 \mu\text{m}$.

In what follows, we present results obtained with the conjugate gradient method (Equations (6) and (7)) and 2D synthetic-DIC images. At each iteration of the method the cost function was evaluated from (5), and it was used as one of the criteria for convergence. The method stops iterating if both the cost function and the estimated parameters have not changed compared to their values at the previous iteration. The method also terminates if it cannot evaluate a possible direction in which the cost function decreases. For the results shown below, the method ran anywhere from 100 to 1000 iterations depending on the phantom and the number of diversity images, K , used for the reconstruction. The method takes about 15 minutes per 100 iterations for $K = 1$, and about 1 hour per 100 iterations for $K = 4$ on a Silicon Graphics processor (SGI R10000). Reconstructions were obtained for $K = 1$ using an image with the direction of shear along the horizontal axis, $K = 2$ using images at 90-degree shear rotations, $K = 4$ with 90-degree shear rotations, and $K = 8$ with 45-degree shear rotations.

5. RESULTS

Our results so far have been encouraging as the conjugate gradient method described here has successfully estimated 2D phase images from synthetic-DIC images computed from computer-generated phantoms, and obtained significant increase in resolution compared to the unprocessed synthetic-DIC images. Reconstructions of a uniform disc with relative phase $\phi = 0.73$ radians (Figure 2a), were computed using progressively fewer synthetic-DIC images (Figure 2b-e and Figure 3). The estimated phase computed using two or more ($K > 1$) synthetic-DIC images is quantitatively better than the one obtained from a single DIC image particularly along the horizontal axis (which

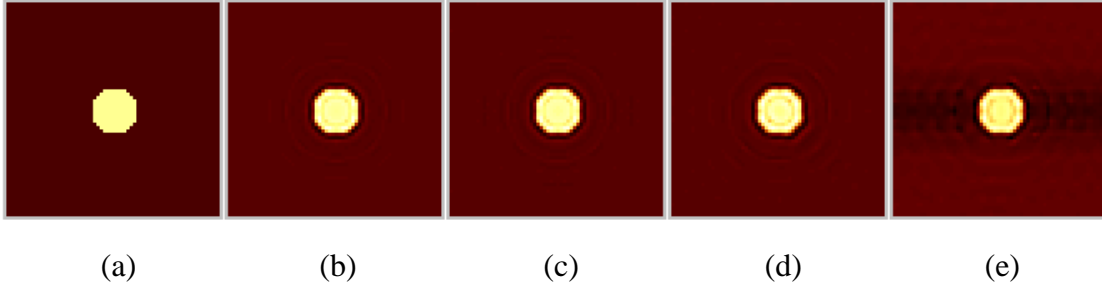


Figure 2: Phase image of a disc with uniform refractive index ($n_1 = 1.56$) embedded in a medium with refractive index $n_2 = 1.52$ (a), and reconstructed phase images computed from the rotational-diversity images shown in Figure 1: (b) from 8 images ($K = 8$); (c) from four images ($K = 4$) with 90-degree shear rotation; (d) from two images ($K = 2$) with orthogonal shear rotation; and (e) from a single image ($K = 1$). The apparent octagon appearance rather than that of a disc is due to the relatively coarse grid used for these studies. Pixels are one value or the other depending on whether the center of the pixel is inside or outside the disc radius. This effect is accentuated here because of the regular pattern of the circle and could be reduced by using smaller pixels.

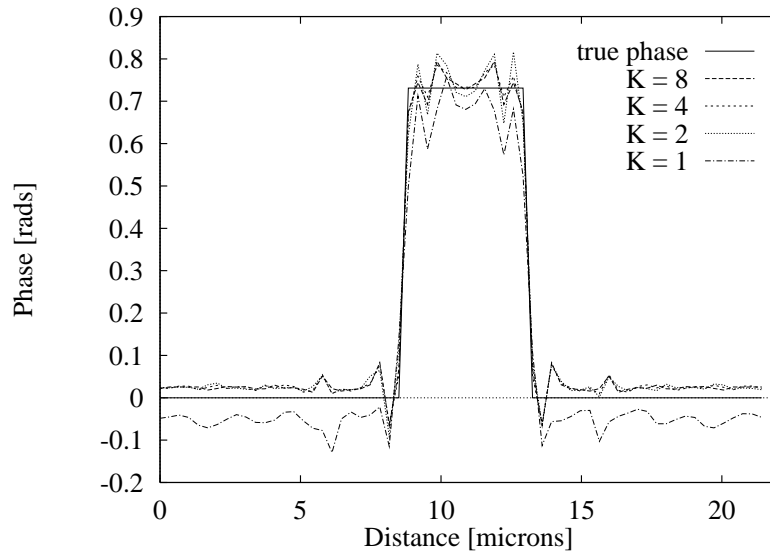


Figure 3: Horizontal profiles through the center of the true phase or “truth” image and the reconstructed phase images of Figure 2. The observed overshoot and undershoot around the sharp edges of the disc, is approximately 9% of the true phase value which is consistent with the Gibbs phenomenon (see Bracewell,¹⁹ p.209).

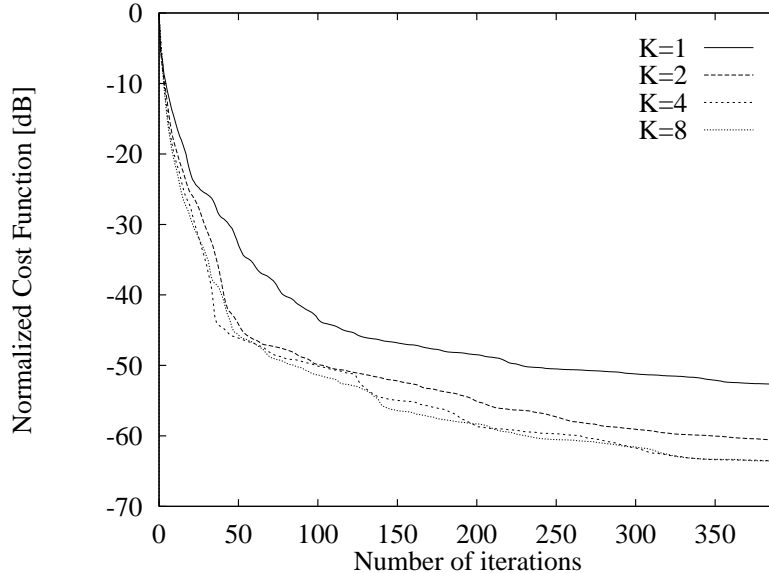


Figure 4: Comparison of the cost function evaluated at every iteration during the estimation of the phase images shown in Figure 2. In each case the cost function was normalized by its value at the first iteration, and then converted to dB (dB value = $10 \log_{10}(\cdot)$).

is the direction of shear in the single DIC image used for the reconstruction) as evident in Figure 3. Overall, reconstructions obtained using two or more images are similar with slight improvement in the match between the reconstruction and the true phase as images at additional rotation angles are included in the reconstruction. In general, only relative phase (or phase difference) can be estimated and thus, the initial guess, ϕ_0 , used in (6) affects the estimated absolute phase value.

In order to demonstrate further the effect of using rotational-diversity DIC images for the phase reconstruction, we compare the cost function evaluated at each iteration for each of the reconstructed images (Figure 4). The cost function decreases more rapidly when two or more ($K > 1$) rotational-diversity images are used compared to reconstruction from a single image. The cost function computed for four and eight images converges to the same value after about 350 iterations and it is approximately 3 dB and 11 dB less than the cost function for two images and one image respectively. Typically, as the number of K increases, the number of iterations required decreases. Examination of the reconstructed phase images every 100 iterations showed small improvements after the first 100 iterations. On the order of 100 to 200 iterations may be adequate for some applications.

Similar results were obtained from synthetic-DIC images (Figure 5) of a “cross” computer-generated phantom with relative phase $\phi = 0.114$ radians (shown in Figure 6 and Figure 7). Because the cross consists of two orthogonal bars, the rotational-diversity DIC images of the cross vary considerably. As expected, the estimated phase from a single DIC image with the direction of shear along the horizontal axis (Figure 5a) is less accurate than phase images computed from two or more DIC images. This is due to fact that there is not enough information about the cross’ horizontal bar in that single DIC image. As in the case of the disc phantom, the reconstructed phase images computed from two or more rotational-diversity DIC images are similar and closely resemble the true values of relative phase (Figure 7). Although it is possible to guess that the actual phantom pattern is a cross from the images in Figure 5, Figure 6b leaves no doubt; it is clearly a cross with approximately constant phase on a background of approximately constant phase.

Results shown in Figures 1 through 6, demonstrate the ability of our method to reconstruct phase from DIC images by reversing the effect of DIC imaging. Clearly the estimated phase images are a better representation of the true phase image than the unprocessed DIC images, and are not direction sensitive as the unprocessed DIC

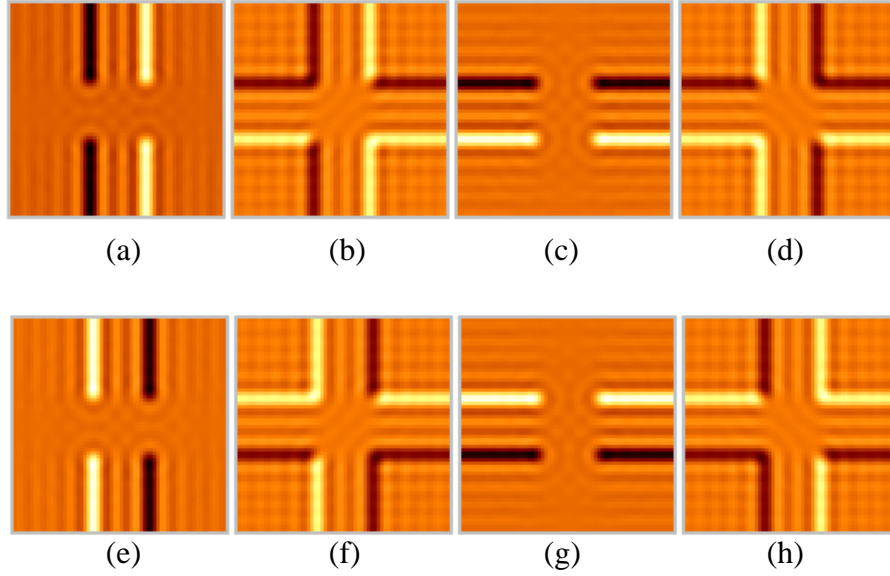


Figure 5: Synthetic rotational-diversity DIC images of a cross with uniform refractive index ($n_1 = 1.504$) embedded in a medium with refractive index $n_2 = 1.494$, with different orientation of the shear. The shear is along the horizontal axis in (a), and it is rotated every 45 degrees clockwise from (a) to (h).

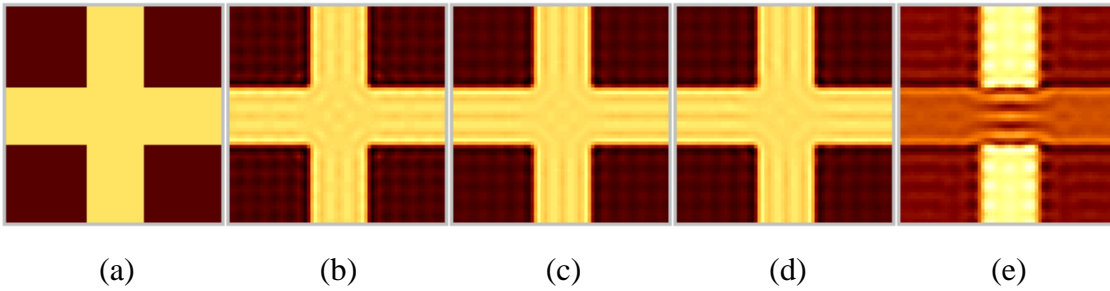


Figure 6: Phase images of a cross with uniform refractive index ($n_1 = 1.504$) embedded in a medium with refractive index $n_2 = 1.494$ (a), and estimated phase obtained from the diversity images shown in Figure 5: (b) from eight images; (c) from four images with 90-degree shear rotation; (d) from two images with orthogonal shear direction; and (e) from a single image.

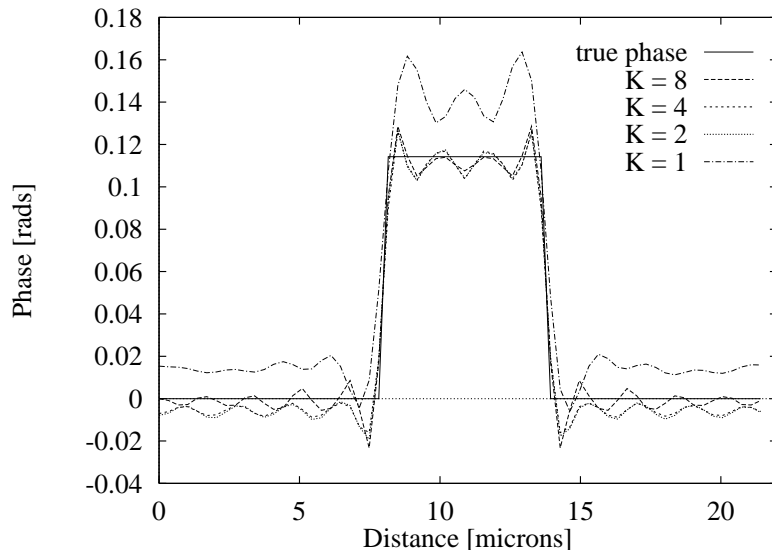


Figure 7: Horizontal profiles through the images in Figure 6. The profiles are taken approximately 1/3 of the distance from the top of the images. The observed overshoot and undershoot is approximately 12%.

images.

5.1. Resolution Test

In order to assess the attainable resolution in estimated phase images reconstructed from rotational-diversity DIC images we have performed a simple simulation. Phase images of a phantom with two points separated by a distance of $0.68 \mu\text{m}$ were computed using the conjugate gradient method. The result shows that two points not resolved in the synthetic-DIC image (Figure 8a) are resolved in the reconstructed phase image when two or more ($K > 1$) DIC images are used (Figure 9, left panel). Furthermore the two points are better resolved when four or more images are used. The benefit of using multiple DIC images in the reconstruction is clearly demonstrated in this simulation. We note that the DIC image of the two-point phantom has the same form as the DIC image of a single point with the same phase difference (Figure 8), and thus it is difficult if not impossible to guess from the unprocessed image that there are two points in the actual phantom. The reconstructed phase images (for $K > 2$) clearly show that there are two distinct points.

Improvement of resolution in reconstructed phase computed from two or more rotational-diversity images is also evident in the reconstructions of a single-point phantom (Figure 9, right panel). The reconstructed point from a single DIC image (Figure 8b) is approximately twice as broad as the point in reconstructions computed from two or more ($K > 1$) DIC images.

6. SUMMARY AND CONCLUSIONS

The derivation of an iterative method that solves the DIC image restoration problem was presented. In our approach we estimate a specimen's phase function using multiple DIC images obtained by rotating the specimen, because DIC imaging is direction sensitive. This *rotational diversity* is a powerful way of obtaining specimen information, because it provides the specimen-phase-function derivative for multiple directions.

The ability of the method to restore the phase function of test objects was demonstrated with results obtained with 2D simulations. Reconstructions computed from one, two, four and eight synthetic-DIC images at different rotation angles more closely resemble the underlying object than the unprocessed DIC images. Our results demon-

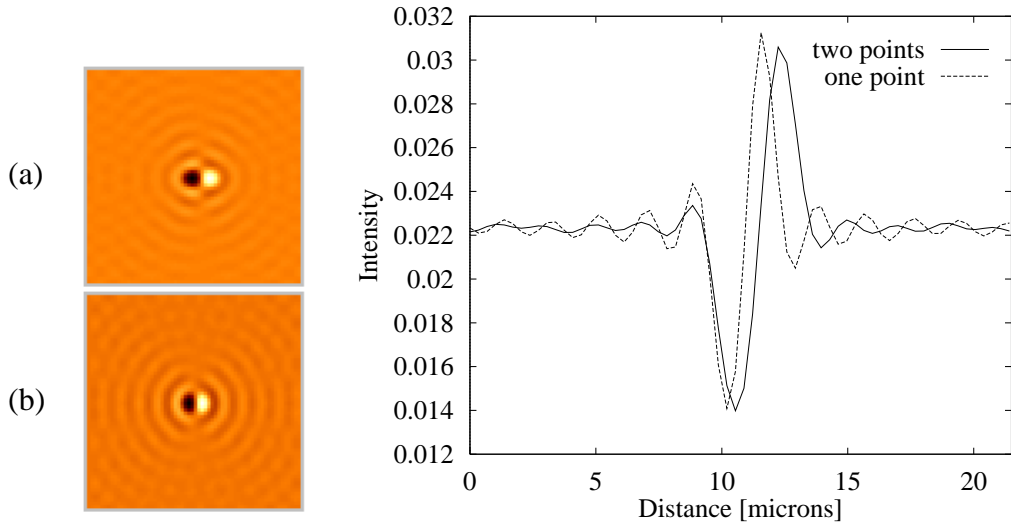


Figure 8: Comparison of synthetic-DIC images generated from the two-point phantom (a), and a single-point phantom (b) with the same relative phase $\phi = 0.8$ radians. Horizontal profiles from center of the two images are compared in the right panel. The direction of shear is along the horizontal axis.

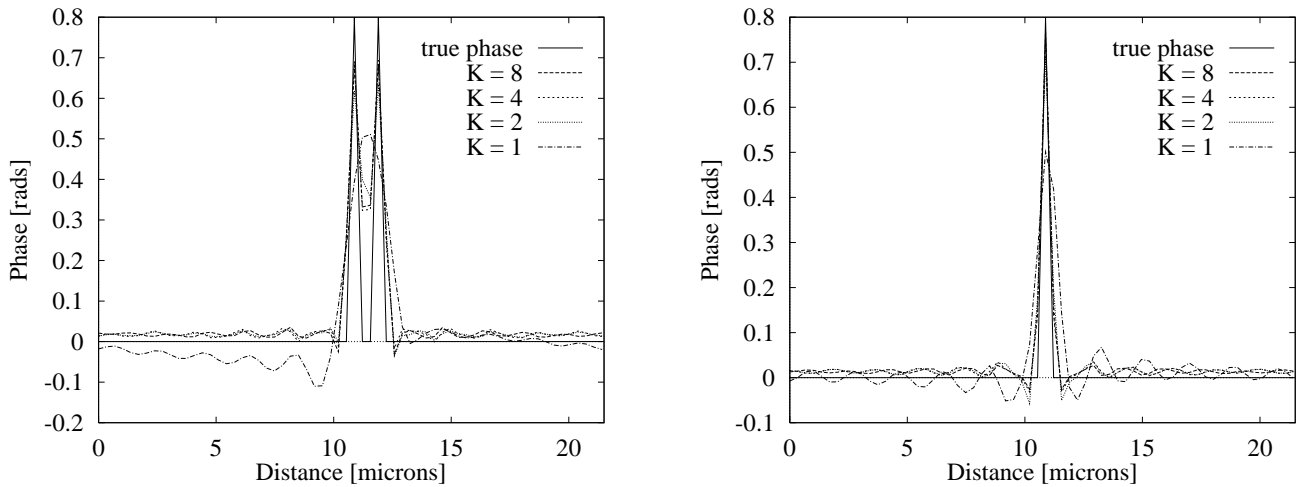


Figure 9: Left panel: Horizontal profiles from the true phase, and reconstructed phase images of the two-point phantom. Right panel: Horizontal profiles from the true phase, and reconstructed phase images of a single-point phantom. The profiles are through the center of the images.

strate that the use of multiple images is very beneficial because the reconstructed phase images are quantitatively better and resolution is improved when two or more DIC images are used in the reconstruction. Improvement in resolution was demonstrated with the reconstruction of two points separated by half the Rayleigh resolution limit for coherent illumination. Although, the two points were not resolved in the unprocessed DIC image, they were successfully resolved in the reconstructed phase images.

Although extremely promising, the 2D phase image results above represent only a preliminary step because they are based on several simplifying assumptions and conditions that would not be true for reconstruction from actual DIC data: 1, precise knowledge of the image formation process; 2, precise knowledge of the shear angle; 3, precise knowledge of the bias; 4, a point condenser aperture; and 5, exact alignment of the DIC images at differing shear angles. Future work includes evaluation of the sensitivity of the reconstruction method to deviation from the ideal conditions used in the simulations presented here, and application of the method to measured DIC images.

7. ACKNOWLEDGEMENTS

This research was supported in part by the National Institutes of Health under research grant No. RR 01380. The authors wish to thank Dr. Fred Rosenberger, and Ms. Joanne Markham for insightful discussions.

8. REFERENCES

- [1] W. Lang. "Nomarski Differential Interference Contrast Microscopy". *A Collection of Four Articles from Zeiss Information, Carl Zeiss, 7082 Oberkochen, West Germany*, 1968.
- [2] H. Gundlach. "Phase Contrast and Differential Interference Contrast Instrumentation and Applications in Cell, Developmental, and Marine Biology". *Optical Engineering*, 32(12):3223–3228, 1993.
- [3] K. R. Spring. "Quantitative Imaging at Low Light Levels: Differential Interference Contrast and Fluorescence Microscopy Without Significant Light Loss". In B. Herman and K. Jacobson, editors, *Optical Microscopy for Biology*, pages 513–522. Wiley-Liss, Inc., New York, NY, 1990.
- [4] J. K. Foskett. "Simultaneous Nomarski and Fluorescence Imaging During Video Microscopy of Cells". *American Journal of Physiology*, 255:C566–C571, 1988.
- [5] M. Pluta. *Advanced Light Microscopy: Specialized Methods*, pages 146–197. Elsevier, Amsterdam, 1989.
- [6] C. Preza, D. L. Snyder, and J.-A. Conchello. Imaging Models for Three-Dimensional Transmitted-Light DIC Microscopy. In *Proceedings of the IS&T/SPIE symposium on Electronic Imaging, Science and Technology*, volume 2655, pages 245–257, 1996.
- [7] T. J. Holmes and W. J. Levy. "Signal-Processing Characteristics of Differential-Interference-Contrast Microscopy". *Applied Optics*, 26(18):3929–3939, 1987.
- [8] T. J. Holmes. "Signal-Processing Characteristics of Differential-Interference-Contrast Microscopy. 2: Noise Considerations". *Applied Optics*, 27(7):1302–1309, 1988.
- [9] R. W. Gerchberg and W. O. Saxton. "A Practical Algorithm for the Determination of Phase from Image and Diffraction Plane Pictures". *Optik*, 35:237, 1972.
- [10] K. Dana. "Three Dimensional Reconstruction of the Tectorial Membrane: An Image Processing Method Using Nomarski Differential Interference Contrast Microscopy". Master's thesis, Massachusetts Institute of Technology, Massachusetts, 1992.
- [11] J. W. Goodman. *Introduction to Fourier Optics*. McGraw-Hill Book Company, New York, 1968.
- [12] J. H. Seldin and R. G. Paxman. Phase-Diverse Speckle Reconstruction of Solar Data. *Proceedings of the SPIE*, 2302-19:268–280, 1994.

- [13] R. G. Paxman, T. J. Schulz, and J. R. Fienup. “Joint Estimation of Object and Aberrations by Using Phase Diversity”. *Journal of the Optical Society of America A*, 9(7):1072–1085, 1992.
- [14] V. Y. Ivanov, V. P. Sivokon, and M. A. Vorontsov. “Phase Retrieval From a set of Intensity Measurements: Theory and Experiment ”. *Journal of the Optical Society of America A*, 9(9):1515–1524, 1992.
- [15] E. Lantz. “Retrieval of a Phase-and-Amplitude Submicrometric Object From Images Obtained in Partially Coherent Microscopy ”. *Journal of the Optical Society of America A*, 8(5):791–800, 1991.
- [16] N. Baba, H. Tomita, and N. Miura. “Iterative Reconstruction Method in Phase-Diversity Imaging ”. *Applied Optics*, 33(20):4428–4433, 1994.
- [17] M. Aoki. *Introduction to Optimization Techniques*. The Macmillan Company, New York, 1971.
- [18] M. Pluta. *Advanced Light Microscopy: Principles and Basic Properties*. PWN - Polish Scientific Publishers, Warszawa, 1988.
- [19] R. N. Bracewell. *The Fourier Transform and Its Applications*. The McGraw-Hill Book Company, New York, 1978.